Shape coexistence and neutron skin thickness of Pb isotopes by the deformed relativistic Hartree-Bogoliubov theory in continuum

Seonghyun Kim, Myeong-Hwan Mun, and Myung-Ki Cheoun*
Department of Physics and Origin of Matter and Evolution of Galaxy (OMEG) Institute, Soongsil University, Seoul 156-743, Korea

Eunja Ha
Department of Physics, Hanyang University, Seoul 04763, Korea

(Received 22 December 2021; accepted 18 March 2022; published 29 March 2022)

We investigate ground states properties of Pb isotopes located between neutron and proton drip-lines estimated by two-neutron (two-proton) separation energies and Fermi energies within the deformed relativistic Hartree-Bogoliubov theory in continuum. First, we report some candidates of nuclear shape coexistence in the isotope chain. They are accessed by calculating total energy as a function of the deformation parameter β_2, and for the coexistence candidates we take a few deformation regions bringing about minima of the energy within energy difference $\Delta E < 1$ MeV. Second, the Pb isotopes near neutron drip-lines are also investigated and compared to the results by other nuclear mass models. We find out 11 neutron emitters, $^{278-296,300}$Pb, giving rise to the Pb peninsular near the neutron drip-line. Finally, by exploiting the neutron and proton density we deduce the neutron skin thickness (NST) of the Pb isotopes and compare to the available experimental data. The recent reports regarding the shape coexistence of ^{184,186,188}Pb and the NST of ^{208}Pb are shown to be well matched with the present results.

DOI: 10.1103/PhysRevC.105.034340

I. INTRODUCTION

The recent development of microscopic nuclear models enables us to predict many intriguing properties of unstable nuclei far from the β-stability region, such as nucleon drip-lines, shape coexistence, nuclear bubble structures, and so on. In particular, the shape coexistence in heavy [1–4] and superheavy nuclei [5] hints important at information of nuclear shapes deeply associated with nuclear deformation and nuclear rotational band structure. The nuclear deformation is also intimately related to the surface symmetry energy in the low density region which also affects the symmetry energy in the high density region like compact astrophysical objects through the first derivative of the symmetry energy [6].

The shape coexistence is being extensively discussed through many theoretical nuclear models and experiments [3–5]. For example, in the nuclei having neutron number $N = 20$ and 28, two-particle two-hole ($2p$-$2h$) configurations of neutrons are shown to be capable of inducing a coexistence shape of some 0^+ states and may give rise to the inversion of island near the neutron drip-line of $N = 20$ nuclei, which enables us to explain the collapse of the magic number of $N = 28$ due to the deformation in the structure of ^{43}S [7]. For heavy nuclei, such as ^{184,186}Pb isotopes, two-quasiparticle and four-quasiparticle configurations by protons may also cause such coexistence [8,9]. Indeed, the energy spectrum of ^{186}Pb shows such shape coexistence due to the β_2 deformation, by which most of the experimental rotational band structures of ^{186}Pb can be understood qualitatively [9].

Drip-lines of the proton and neutron of heavy nuclei are also interesting because they are closely associated with the nuclear emitter of protons and neutrons far from the β stability region. We access the separation energies of neutrons and protons of the nuclei, by which one can list the proton and/or neutron emitter of the nuclei. All of these properties are known to be sensitive to the deformation of the nuclei as discussed in the nuclear mass models [10–12].

Concurrently, neutron skin thickness (NST) of ^{208}Pb becomes one of the important data for understanding the heavy nuclear structure as well as neutron star properties. Recent data from PREX II [13,14] demonstrated more clear data of the NST of ^{208}Pb as $R_{\rm skin} = (0.283 \pm 0.071)$ fm, which is a much more precise value rather than PREX I data [15,16]. It could rule out many nuclear models with the neutron star data by the recent gravitational wave data and x-ray observational data. Therefore direct calculations of the NST might be a prerequisite for investigating the validity of these nuclear models before the application to the interesting topics in nuclear astrophysics. This paper is organized as follows. In Sec. II, we briefly summarize the basic formalism used in the present calculation. Detailed results for the shape coexistence, separation energies and NSTs for Pb isotopes are provided in Sec. III. Finally summary and conclusion are done in Sec. IV.

II. FORMALISM

In order to consider the above discussions we need a well-refined nuclear model which has to incorporate the

*cheoun@ssu.ac.kr

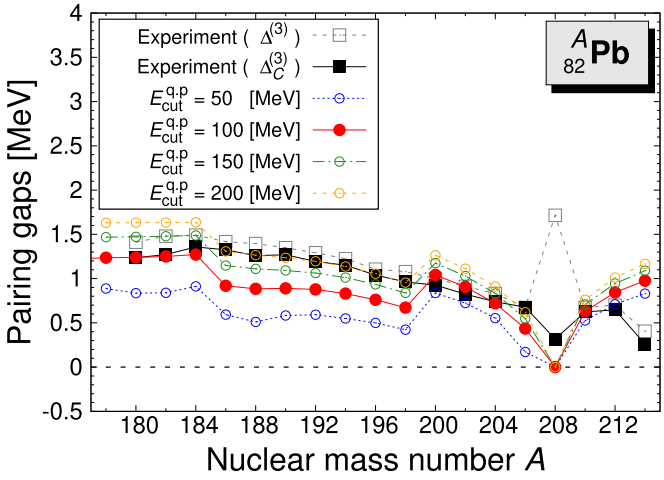

FIG. 1. Neutron pairing gaps of Pb isotopes ($A = 186$–198) with respect to the pairing window denoted as $E_{\rm cut}^{q.p.}$. Empirical pairing gaps are obtained by the three-point binding energies, $\Delta^{(3)}$ and $\Delta_C^{(3)}$, which are taken from Refs. [39,40], respectively. The latter formula includes the shell corrections for the nucleon magic numbers.

deformation, the pairing correlations, and the continuum through the microscopic approach and explain the whole nuclear masses covering nuclei near drip lines. Another important ingredient is the relativistic description which has been initiated by the authors in Refs. [17,18] with various meson-exchange models inside nuclei and has enabled us to incorporate consistently nucleonic spin degree of freedom.

Along this line the deformed relativistic Hartree-Bogoliubov theory in continuum (DRHBc) was developed for deformed halo nuclei in Refs. [19,20] and recently extended [21] with point-coupling density functionals. This theory is proved to be capable for a nice description of the nuclear mass with highly predictive power [22,23] and successfully applied to some nuclei [24–31], which followed the previous relativistic continuum Hartree-Bogoliubov (RCHB) approach calculated in coordinate space [32,33] by explicitly including the deformation in a Dirac Woods-Saxon basis [34]. Here, we note that the deformed cylindrical basis preserving axial symmetry could be an alternative to effectively treat the convergence of total energy as argued in Ref. [35], where the Gogny-type pairing force was exploited for neutron rich nuclei near the drip line and odd nuclei.

In this work, we focus on the shape coexistence and NST of the Pb isotopes within the DRHBc theory, which was succinctly summarized in Refs. [20,21]. The present calculations are carried out in the following relativistic Hartree-Bogoliubov theory with the density functional PC-PK1 [36],

$$\begin{pmatrix} h_D - \lambda & \Delta \\ -\Delta^* & -h_D + \lambda \end{pmatrix} \begin{pmatrix} U_k \\ V_k \end{pmatrix} = E_k \begin{pmatrix} U_k \\ V_k \end{pmatrix}, \tag{1}$$

where h_D, λ, E_k, (U_k, V_k) are the Dirac Hamiltonian, the Fermi energy, and the quasiparticle energy and wave function,

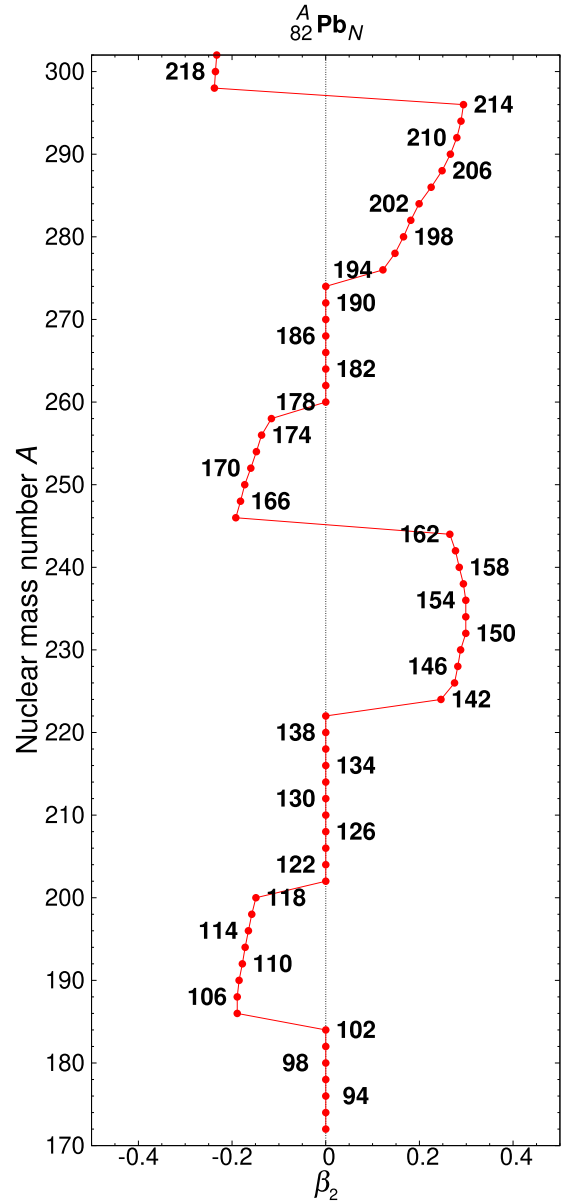

FIG. 2. Deformation parameter β_2 determined by the minimum of total (ground state) binding energy calculated by DRHBc model for the nuclei from ^{172}Pb up to ^{302}Pb isotopes having a neutron number $N = 90$–220 considered in this work. Thick letters stand for neutron number.

respectively. The paring potential Δ is given with the pairing tensor $\kappa(\mathbf{r}, \mathbf{r}')$ as follows:

$$\Delta(\mathbf{r}, \mathbf{r}') = V(\mathbf{r}, \mathbf{r}')\kappa(\mathbf{r}, \mathbf{r}') \tag{2}$$

with a density-dependent zero range force

$$V(\mathbf{r}, \mathbf{r}') = \frac{V_0}{2}(1 - P_\sigma)\delta(\mathbf{r} - \mathbf{r}')\left(1 - \frac{\rho(\mathbf{r})}{\rho_{\rm sat}}\right). \tag{3}$$

For the pairing strength, we use $V_0 = -325.0$ MeV fm^3. The saturation density is adopted as $\rho_{sat} = 0.152$ fm^{-3} together with a pairing window of 100 MeV. The energy cutoff

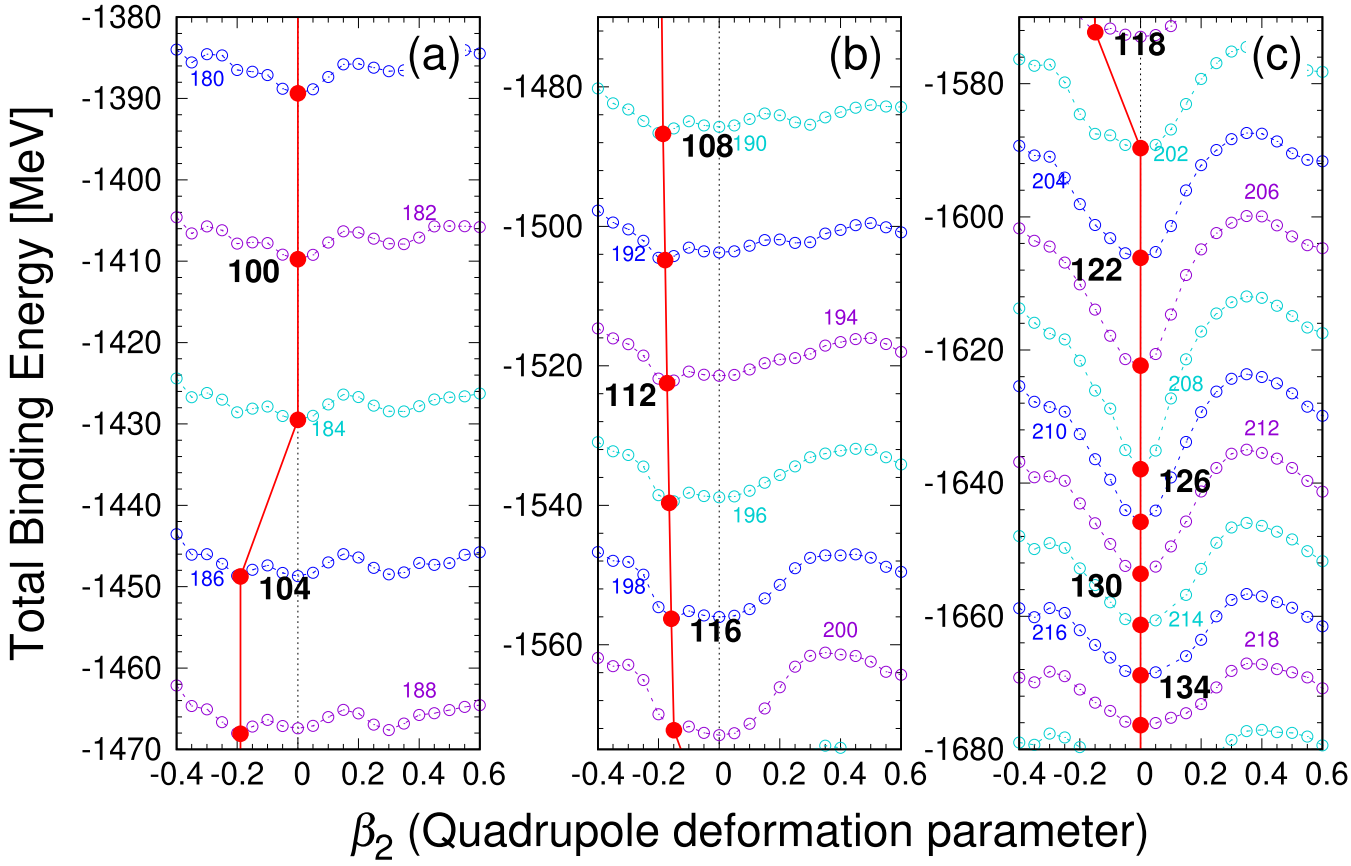

FIG. 3. Evolution of total binding energy of $^{180–188}$Pb (a), $^{190–200}$Pb (b), and $^{202–218}$Pb isotopes (c) with the β_2 deformation. Thick (thin) letters stand for neutron (total mass) number.

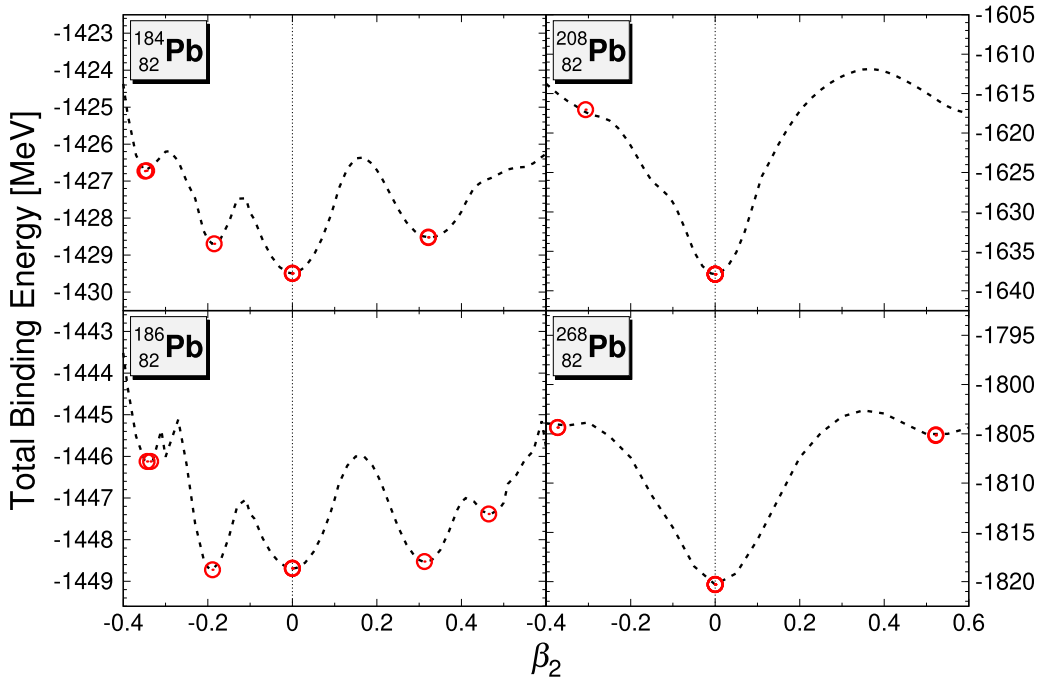

FIG. 4. Detailed energy evolutions of ^{184,186,208,268}Pb isotopes for given β_2 deformations, which show a couple of deformation regions having almost the same total binding energy minima for ^{184,186}Pb. They are compared to the spherical double magic nuclei ^{208,268}Pb. Not only global minima but also local minima points have been denoted by red circles.

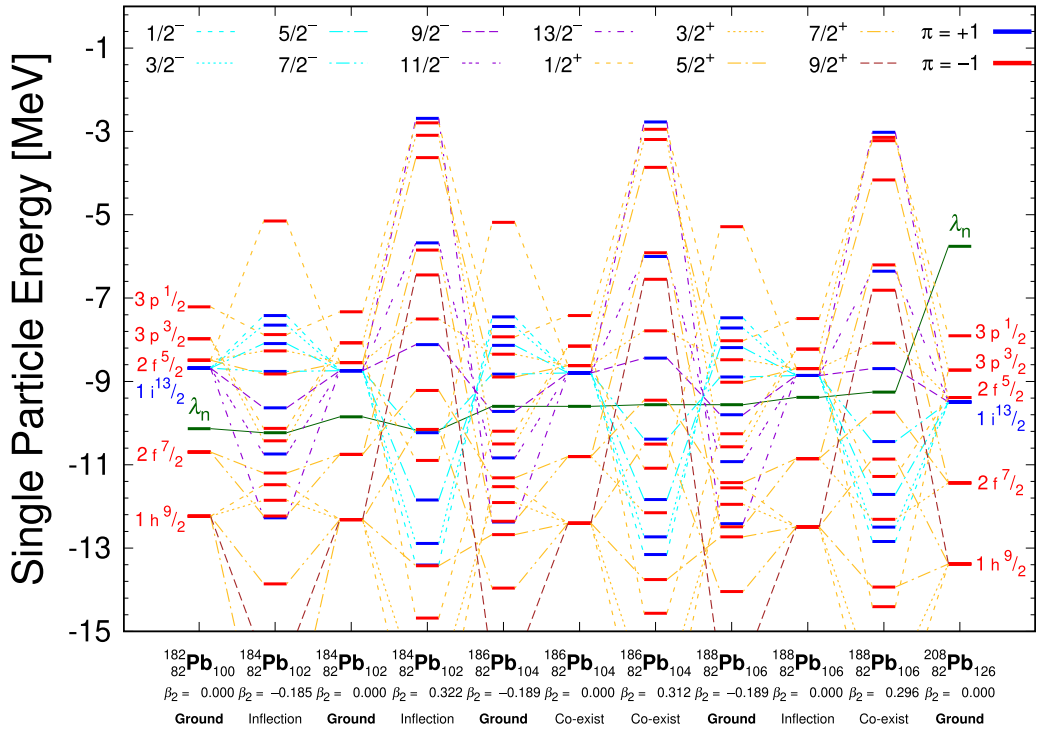

FIG. 5. Neutron SPS evolutions of ^{184,186,188}Pb isotopes for the shape coexistence: oblate, spherical, and prolate cases. For reference, the SPS for ^{182,208}Pb are also shown in the leftmost and rightmost columns, respectively. Fermi energies of neutron (λ_n) are also shown for illustrating the shape coexistence.

$E^{+}_{\rm cut} = 300$ MeV and the angular momentum cutoff $J_{\rm max} = (23/2)\hbar$ are taken for the Dirac Woods-Saxon basis. The above numerical details are the same as those suggested in Refs. [21,23] for the DRHBc mass table calculation. For the present Pb isotopes, the Legendre expansion truncation is chosen as $\lambda_{\rm max} = 8$ [21,23].

Empirical pairing gaps of Pb isotopes were shown to be properly reproduced with the energy cutoff, the maximum angular momentum and the Legendre expansion truncation obtained from the convergence check of total energies as shown in Fig. 5(b) in Ref. [21].

The present zero-range scheme for the pairing force is better than the simple constant gap approximation, but it has still the pairing window problem in the pairing tensor as discussed in Refs. [37,38] because it needs an arbitrary energy cut off parameters for neutron-rich nuclei. Figure 1 shows that, in spherical nuclei, the neutron pairing gaps are well reproduced by the pairing window denoted as $E^{q.p}_{\rm cut} = 100$ MeV. But for deformed nuclei $A = 186$–198 (see Fig. 2) the results by $E^{q.p}_{\rm cut} = 200$ MeV are better than those by other windows. It infers that the convergence of total energies with the pairing energies is to be deliberately examined for deformed nuclei. We leave it as a future work because we need to study the masses of odd nuclei by the present DRHBc model for systematically deducing the theoretical pairing gaps. A more elaborate approach for the pairing interaction beyond the zero-range scheme is to use the Gogny-type finite-range pairing force [41] using a separable approximation [42,43]. This kind of treatment of pairing interaction is also applied to the covariant density-functional-theory (DFT) adopted for studying neutron rich nuclei in Refs. [44–47].

III. RESULTS AND DISCUSSIONS

In Fig. 2, we illustrate the β_2 deformation of $^{172\text{–}302}$Pb isotopes obtained by the minimum of the total binding energy calculated from the DRHBc framework. First, we note that there are three spherical nuclei region around $N = 100$, 126, and 184. In particular, it is remarkable that $N = 100$ might be a candidate for submagic shell which is occupied up to $2f_{7/2}$ shell because the nuclei around $N = 100$ disclose spherical shapes similarly to those nuclei in the vicinity of $N = 126$ and 184. The neutron-deficient Pb isotopes show oblate deformations after the spherical shapes near $N \sim 100$ region, and the isotopes near stability lines are settled down to the spherical type around $N \sim 126$ region filled up to $3p_{1/2}$ shell. The isotopes of the neutron-rich side go to prolate until ^{244}Pb by the prolate subshell $N = 162$ region and move to the oblate region by the oblate subshell $N = 172$ and 178 in the Nilsson diagram [48]. After that the Pb isotopes go back to spherical region owing to the magic number $N = 184$ region and the isotopes near neutron drip-line settle down to the prolate shape, apart from ^{298,300,302}Pb.

In Fig. 3, we detail the total binding energy evolution in some specific mass region $180 \leqslant A \leqslant 218$ in terms of the deformation parameter β_2, which shows the shape transition from spherical to oblate deformation. In the $186 \leqslant A \leqslant 200$ region, the oblate shape appears. These oblate shapes are

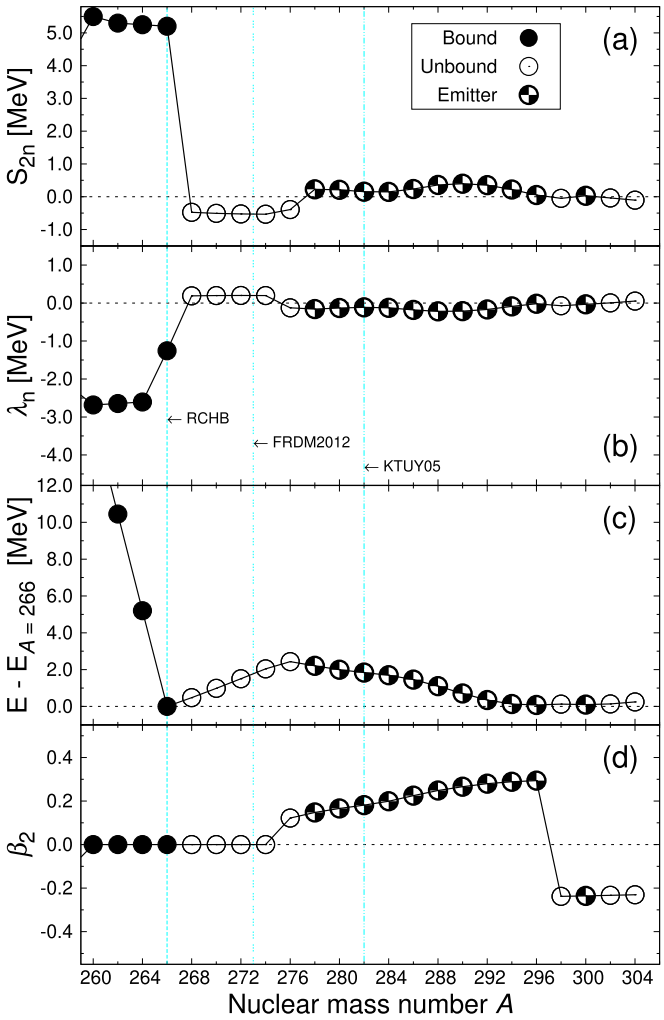

FIG. 6. Two-neutron separation energies (S_{2n}) (a), Fermi energies (λ_n) (b), relative energy with respect to the doubly magic nucleus, ^{266}Pb, (c), and deformation parameter (β_2) (d) of Pb isotopes near the neutron-drip region.

thought to come from the valence neutrons and holes between $N = 100$ (fulfilled up to the $1h_{9/2}$ and $2f_{7/2}$ shells) and $N = 126$ (up to the $2g_{9/2}$ shell). This fact is discussed with the evolution of single-particle states (SPS) for Pb isotopes later on. Here, we note that the present DRHBc model was applicable for the nuclear mass table [21] and the mass table of the even-even nuclei is in preparation for publication [49]. In particular, ^{184,186}Pb were claimed to show a typical shape coexistence [8,9]. The total binding energy curve for ^{184,186,188}Pb in Fig. 3(a) also displays the possibility of the shape coexistence.

In Fig. 4, we detail the precise total binding energy surfaces of ^{184,186}Pb and ^{208,268}Pb. The former nuclei have been being discussed for their coexistence nuclear shapes [9] and the latter are shown for testing the present model for the well-known spherical nuclei. As shown in the left panels of Fig. 4, the results of ^{184,186}Pb disclose a possibility of the shape coexistence of oblate, spherical, and prolate shapes depending on the β_2 deformation, whose energy differences are within 1 MeV. We note that the energy difference in the coexistence of ^{186}Pb is a bit smaller than that of ^{184}Pb. The feasible coexistence of ^{184,186}Pb by the oblate and prolate deformation as well as the spherical type could be a precursor of the yrast states of the rotational bands discussed in Ref. [9]. Right panels in Fig. 4 show the spherical minima of the total binding energy surfaces of ^{208,268}Pb near the magic number $N = 126$ and 184 coming from the double magic nucleus.

The present results for the shape coexistence can be understood by the neutron SPS evolution along with the deformation in Fig. 5, where the SPS evolution of three isotopes ^{184,186,188}Pb is displayed with those of the spherical ^{182,208}Pb isotopes, which have a submagic $N = 100$ and a magic $N = 126$ number, respectively, in the leftmost and rightmost columns. One can note that the three isotopes have almost the same neutron Fermi energies (λ_n) for oblate, spherical, and prolate cases. In particular, we confirm ^{184,186}Pb as the feasible coexistence nuclei because the nuclei have oblate and prolate as well as spherical minimum energies with $\Delta E < 1$ MeV. We note that ^{188}Pb might also be the candidate of the shape coexistence as discussed by the interacting boson model [50].

This shape coexistence is thought to come from the deformation. The two, four, and six valence neutrons in the $1i_{13/2}$ shell above the core by the submagic number $N = 100$ (occupied up to the $1h_{9/2}$ and $2f_{7/2}$ shells) are allocated to many projection states split from the $1i_{13/2}$ shell due to the deformation. For the prolate case, the lower $1/2^-$–$7/2^-$ (higher $11/2^-$–$13/2^-$) projection states of the $1i_{13/2}$ state are shifted to the lower (higher) energy states, as shown in the blue (purple) color system. The shifts are reversed for the oblate case. This shift of the projection states by the deformation is very general in the Nilsson diagram [51]. As a result, both low and high energy splitting effects by the deformation are compensated with each other and give rise to almost the same Fermi energies within $\Delta E < 1$ MeV leading to the shape coexistence.

The conventional understanding of the shape coexistence is the lowering of the proton particle-hole (p-h) excitation for quasiparticles due to the interaction of the proton-particle with neutron-hole near the closed magic $N = 126$ core [52]. Although we do not calculate the nuclear excitation in the present work, if we treat $N = 100$ as a kind of submagic shell salient in the spherical case, the additional two or four neutrons above the submagic shell might be excited by the $2p$-$2h$ excitation, which may lead to the more clear shape coexistence. This coexistence near the submagic $N = 100$ number might resemble the coexistence of spherical and deformed shape in ^{43}S in the vicinity of the $N = 28$ magic number [53] leading to the collapse of the $N = 28$ magic number [7].

Hereafter we discuss the neutron drip-line of Pb isotopes. In Fig. 6, we present two-neutron separation energies (S_{2n}) (a), Fermi energies (λ_n) (b), relative energy with respect to ^{266}Pb (c), and deformation parameter (β_2) (d) of Pb isotopes near neutron drip-line with the most neutron-rich Pb isotope estimated by other nuclear mass models, such as the RCHB [32,33], FRDM [10], and KTUY models [11]. The first point

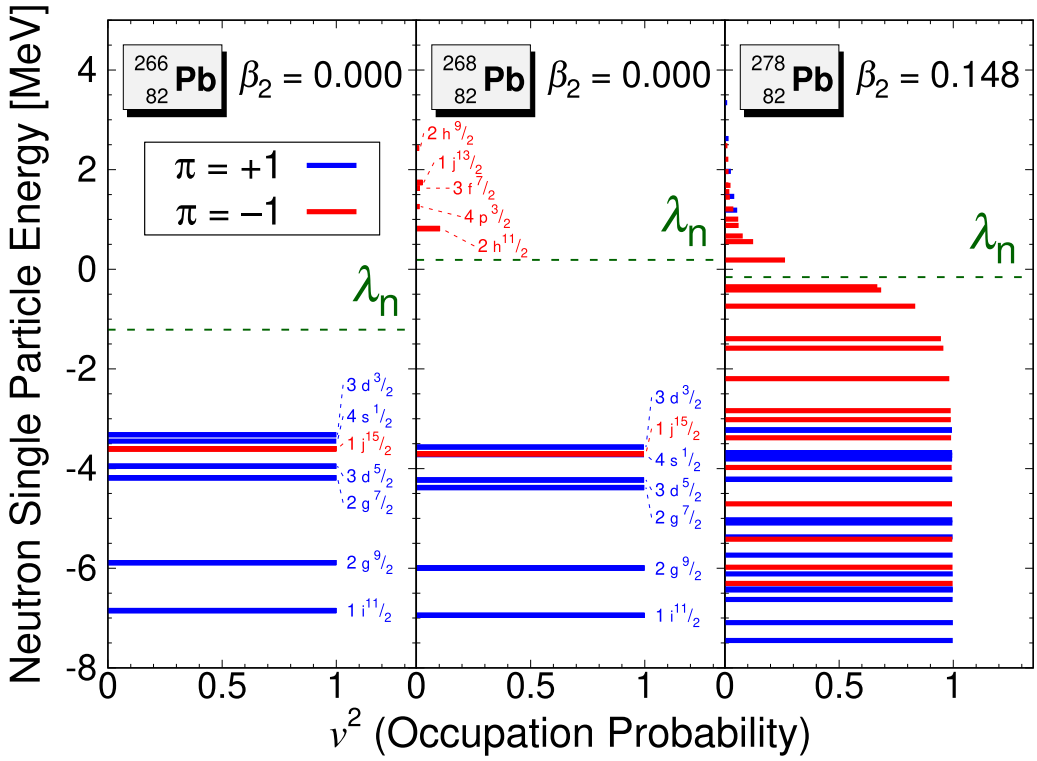

FIG. 7. Neutron SPS occupation probabilities of bound ^{266}Pb, unbound ^{268}Pb, and neutron emitter ^{278}Pb.

to notice is the further extension of the investigation up to ^{304}Pb compared to those of ^{268}Pb by RCHB, ^{272}Pb by FRDM 2012 and ^{282}Pb by the KTUY05 model. This extension is mainly due to the deformation and the continuum states as discussed in Refs. [26,54].

The second point is that there exists some unstable nuclei region from ^{268}Pb to ^{304}Pb, in which the situation is more or less similar to the results of Hs near the neutron drip line as discussed in Fig. 3(a) of Ref. [23], which show three unbound, five neutron emitter, i.e., stable against two-neutron emission but unstable against multineutron emission, with the increase of the neutron number after ^{366}Hs having a neutron magic number $N = 258$. This property has lead to the peninsula of heavy nuclear isotopes of $102 \leqslant Z \leqslant 120$ near neutron drip lines.

In the present Pb isotopes, ^{266}Pb having the magic number of $N = 184$ [48] is treated as a doubly magic nucleus. After ^{266}Pb, ^{268,270,272,274,276}Pb and ^{298,302,304}Pb are unbound [see Fig. 6(a) and 6(b)], while other nuclei $^{278–296}$Pb and ^{300}Pb are unstable against multineutron emission, as shown in Fig. 6(c). It means that $^{278–296,300}$Pb can be neutron emitter nuclei and become a peninsular in the nuclear chart for the $Z = 82$ isotope. This feature can be explained by the occupation probabilities of the Pb isotopes. In Fig. 7, the characteristics of the typical bound, unbound, and neutron emitters, such as ^{266}Pb, ^{268}Pb, and ^{278}Pb, are clearly displayed. The neutrons beyond the doubly magic nucleus are shown to locate in the continuum states, which causes the unbound and neutron emitter nuclei. In particular, the large and small energy difference between the continuum states and the last occupied state leads to the unbound nuclei and the neutron emitter, respectively.

Finally, we show the NST of Pb isotopes. Figure 8 illustrates the density distribution of neutrons and protons for ^{208}Pb. Using the root mean square radius in the distribution we obtain the NST for ^{208}Pb as $R_n - R_p = 0.257$ fm, which is quite well matched with the PREX II experimental data 0.283 ± 0.071 [13] within the confidence level. One interesting point is that the neutron density in the inner core is much larger than that of the proton density and the surface part has also a large neutron density, that is, NST. It implies that the symmetry energy in finite nuclei has the contribution from both volume and surface parts. The surface symmetry energy is to be subtracted from the symmetry energy from finite nuclei for considering the symmetry energy for nuclear matter as argued in Refs. [6,55].

In addition, we illustrate the evolution of charge radii, neutron and proton density, and the NST in Fig. 9. The charge radii obtained in the present work are also well matched with the experimental data. Moreover, it increases with the increase of the neutron number, that is, it is swollen with the increase of the neutron number. Figure 9(c) shows the NST evolution, which monotonically increases along with the neutron number. No special behavior of the NST evolution was not found. But it is remarkable that the NST of ^{246,260}Pb shows a jumping leap from the previous nuclei. This behavior comes from the sudden change of the nuclear shape as shown in Fig. 2. Also there is a kink at $A = 224$, which may be due to the deformation effect.

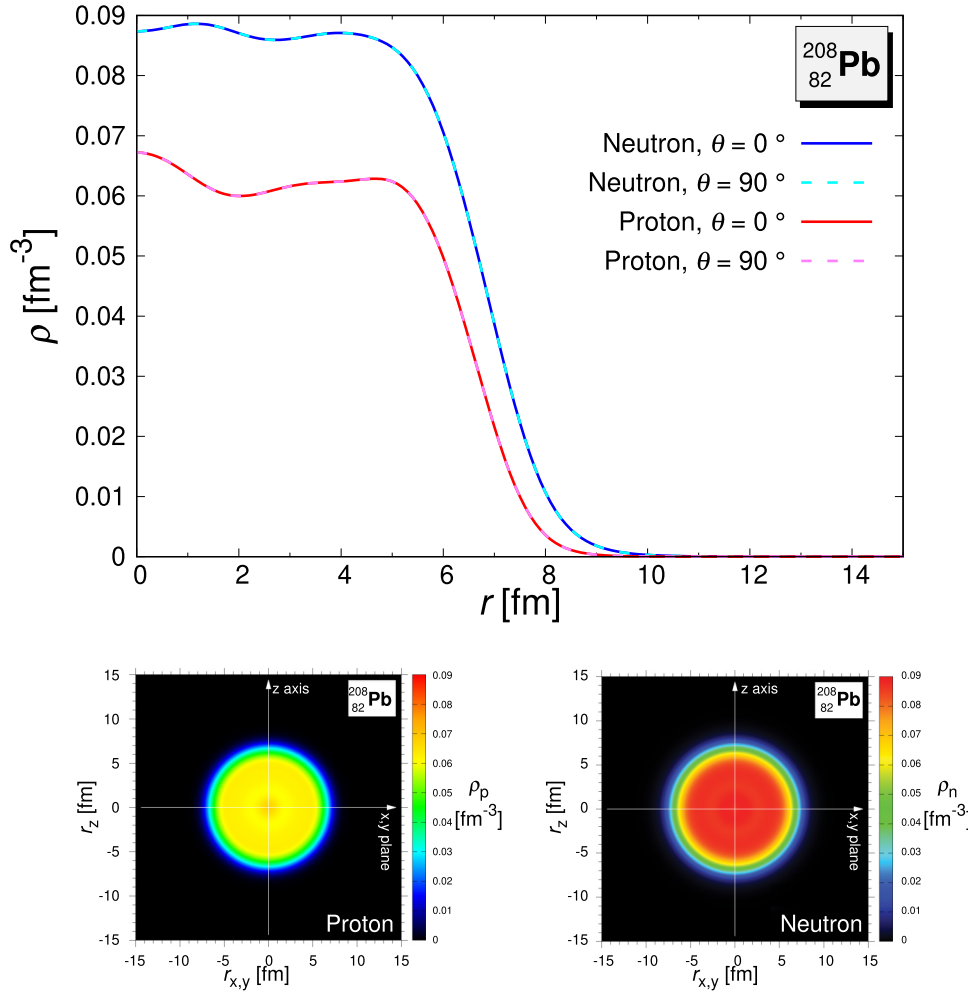

FIG. 8. Upper panel is the neutron (solid line) and proton (dashed line) density distribution for the spherical ^{208}Pb and left (right) lower panel is a bird-eye view of the neutron (proton) density distribution. Since ^{208}Pb is a spherical nucleus, the results for $\theta = 0^\circ$ and 90° are the same.

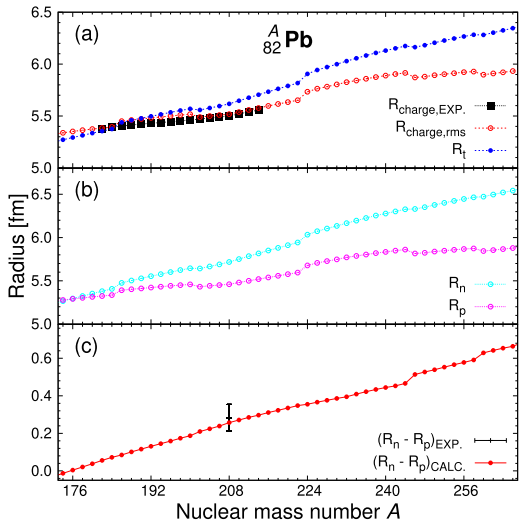

FIG. 9. Evolution of charge radii calculated by the root mean square (rms), where R_t is the mass radii (a), neutron and proton radii (b), and NST (c) for Pb isotopes. Charge radii data in (a) and NST data in (c) are taken from Refs. [13,56], respectively.

IV. SUMMARY AND CONCLUSION

In summary, we calculated the total binding energy of the Pb isotopes in terms of the β_2 deformation using the DRHBc framework. Energy evolutions with the deformation were investigated in detail for those isotopes. We found some shape coexistence candidates in ^{184,186,188}Pb, which are quite consistent with the results from the rotational bands of those nuclei. We also found a peninsula in the vicinity of the neutron drip line due to the neutron emitter after the $N = 184$ closed shell. They stem from the deformation and the continuum states carefully considered in the present model. Finally, the neutron skin thickness of ^{208}Pb is calculated and compared to the recent PREX II data. The results turn out to be quite successful with the reported confidence level. Also the evolution of the NST and the related charge radii are presented for the Pb isotopes.

In conclusion, the DRHBc framework is shown to predict and properly confirm some important nuclear properties, such as nuclear shape coexistence, neutron emitter, and neutron skin thickness, of Pb isotopes. The results of the application to other heavy nuclei will appear elsewhere. Finally,

we note that the pairing gaps for deformed nuclei should be treated more carefully with more a appropriate paring window in the convergence of total energies with the deformation.

ACKNOWLEDGMENTS

Helpful discussions with members of the DRHBc Mass Table Collaboration are gratefully appreciated. This work was supported by the National Research Foundation of Korea (Grants No. NRF-2018R1D1A1B05048026, No. NRF-2020R1A2C3006177, No. NRF-2020K1A3A7A09080134, No. NRF-2021R1F1A1060066, and No. NRF-2021R1A6A1 A03043957). This work was supported by the National Supercomputing Center with supercomputing resources including technical support (KSC-2020-CRE-0329, KSC-2021-CRE-0126, and KSC-2021-CRE-0272).

[1] J. L. Wood and K. Heyde, J. Phys. G **43**, 020402 (2016).
[2] A. Gade and S. N. Liddick, J. Phys. G **43**, 024001 (2016).
[3] K. Heyde and J. L. Wood, Rev. Mod. Phys. **83**, 1467 (2011).
[4] E. Nácher, A. Algora, B. Rubio, J. L. Taín, D. Cano-Ott, S. Courtin, P. Dessagne, F. Maréchal, C. Miehé, E. Poirier, M. J. G. Borge, D. Escrig, A. Jungclaus, P. Sarriguren, O. Tengblad, W. Gelletly, L. M. Fraile, and G. Le Scornet, Phys. Rev. Lett **92**, 232501 (2004).
[5] A. N. Andreyev *et al.*, Nature (London) **405**, 430 (2000).
[6] P. Danielewicz, Nucl. Phys. A **727**, 233 (2003).
[7] P. Mantica, Physics **2**, 18 (2009).
[8] J. Wauters, N. Bijnens, H. Folger, M. Huyse, Han Yull Hwang, R. Kirchner, J. von Schwarzenberg, and P. Van Duppen, Phys. Rev. C **50**, 2768 (1994).
[9] T. Duguet, M. Bender, P. Bonche, and P.-H. Heenen, Phys. Lett. B **559**, 201 (2003).
[10] P. Moeller, A. J. Sierk, T. Ichikawa, and H. Sagawa, At. Data Nucl. Data Tables, **109–110**, 1 (2016).
[11] H. Koura, T. Tachibana, M. Uno, and M. Yamada, Prog. Theor. Phys. **113**, 305 (2005).
[12] D. Lunney, J. M. Pearson, and C. Thibault, Rev. Mod. Phys. **75**, 1021 (2003).
[13] D. Adhikari *et al.*, Phys. Rev. Lett. **126**, 172502 (2021).
[14] B. T. Reed, F. J. Fattoyev, C. J. Horowitz, and J. Piekarewicz, Phys. Rev. Lett. **126**, 172503 (2021).
[15] S. Abrahamyan, Z. Ahmed, H. Albataineh, K. Aniol, D. S. Armstrong *et al.*, Phys. Rev. Lett. **108**, 112502 (2012).
[16] C. J. Horowitz, Z. Ahmed, C.-M. Jen, A. Rakhman, P. A. Souder, M. M. Dalton, N. Liyanage, K. D. Paschke, K. Saenboonruang, R. Silwal, G. B. Franklin, M. Friend, B. Quinn, K. S. Kumar, D. McNulty, L. Mercado, S. Riordan, J. Wexler, R. W. Michaels, and G. M. Urciuoli, Phys. Rev. C **85**, 032501(R) (2012).
[17] J. D. Walecka, Ann. Phys. (NY) **83**, 491 (1974).
[18] J. Boguta and R. Bodmer, Nucl. Phys. A **292**, 413 (1977).
[19] S.-G. Zhou, Jie Meng, P. Ring, and E.-G. Zhao, Phys. Rev. C **82**, 011301(R) (2010).
[20] L. Li, Jie Meng, P. Ring, E.-G. Zhao, and S.-G. Zhou, Phys. Rev. C **85**, 024312 (2012).
[21] K. Zhang, M. K. Cheoun, Y. B. Choi, P. S. Chong, J. Dong, L. Geng, E. Ha, X. He, C. Heo, M. C. Ho, E. J. In, S. Kim, Y. Kim, C. H. Lee, J. Lee, Z. Li, T. Luo, J. Meng, M. H. Mun, Z. Niu, C. Pan, P. Papakonstantinou, X. Shang, C. Shen, G. Shen, W. Sun, X. X. Sun, C. K. Tam, Thaivayongnou, C. Wang, S. H. Wong, X. Xia, Y. Yan, R. W.-Y. Yeung, T. C. Yiu, S. Zhang, W. Zhang, and S. G. Zhou, Phys. Rev. C **102**, 024314 (2020).
[22] C. Pan, K. Y. Zhang, P. S. Chong, C. Heo, M. C. Ho, J. Lee, Z. P. Li, W. Sun, C. K. Tam, S. H. Wong, R. W.-Y. Yeung, T. C. Yiu, and S. Q. Zhang, Phys. Rev. C **104**, 024331 (2021).
[23] K. Zhang, X. He, J. Meng, C. Pan, C. Shen, C. Wang, and S. Zhang, Phys. Rev. C **104**, L021301 (2021).
[24] C. Pan, K. Zhang, and S. Zhang, Int. J. Mod. Phys. E **28**, 1950082 (2019).
[25] X.-X. Sun, J. Zhao, and S.-G. Zhou, Nucl. Phys. A **1003**, 122011 (2020).
[26] E. J. In, P. Papakonstantinou, Y. Kim, and S.-W. Hong, Int. J. Mod. Phys. E **30**, 2150009 (2021).
[27] X.-X. Sun, J. Zhao, and S.-G. Zhou, Phys. Lett. B **785**, 530 (2018).
[28] Z. H. Yang, Y. Kubota, A. Corsi, K. Yoshida, X.-X. Sun, J. G. Li, M. Kimura, N. Michel, K. Ogata, C. X. Yuan, Q. Yuan, G. Authelet, H. Baba, C. Caesar, D. Calvet, A. Delbart, M. Dozono, J. Feng, F. Flavigny, J.-M. Gheller *et al.*, Phys. Rev. Lett. **126**, 082501 (2021).
[29] X.-X. Sun, Phys. Rev. C **103**, 054315 (2021).
[30] X.-X. Sun and S.-G. Zhou, Sci. Bull. **66**, 2072 (2021).
[31] Xiang-Xiang Sun and Shan-Gui Zhou, Phys. Rev. C **104**, 064319 (2021).
[32] J. Meng and P. Ring, Phys. Rev. Lett. **77**, 3963 (1996).
[33] J. Meng, Nucl. Phys. A **635**, 3 (1998).
[34] S.-G. Zhou, Jie Meng, and P. Ring, Phys. Rev. C **68**, 034323 (2003).
[35] L. M. Robledo, R. Bernard, and G. F. Bertsch, Phys. Rev. C **86**, 064313 (2012).
[36] P. W. Zhao, Z. P. Li, J. M. Yao, and J. Meng, Phys. Rev. C **82**, 054319 (2010).
[37] J. Dobaczewski, W. Nazarewicz, T. R. Werner, J. F. Berger, C. R. Chinn, and J. Decharge, Phys. Rev. C **53**, 2809 (1996).
[38] Y. Tian, Z. Y. Ma, and P. Ring, Phys. Lett. B **676**, 44 (2009).
[39] P. Moeller and J. R. Nix, Nucl. Phys. A **536**, 20 (1992).
[40] S. A. Changizi, Chong Qi, and R. Wyss, Nucl. Phys. A **940**, 210 (2015).
[41] J. Decharge and D. Gogny, Phys. Rev. C **21**, 1568 (1980).
[42] M. Serra, A. Rummel, and P. Ring, Phys. Rev. C **65**, 014304 (2001).
[43] T. Niksic, N. Paar, D. Vrentano, and P. Ring, Comput. Phys. Commun. **185**, 1808 (2014).
[44] D. Vretenar, A. V. Afanasjev, G. A. Lalazissis, and P. Ring, Phys. Rep. **409**, 101 (2005).
[45] S. E. Agbemava, A. V. Afanasjev, D. Ray, and P. Ring, Phys. Rev. C **89**, 054320 (2014).
[46] A. V. Afanasjev, S. E. Agbemava, D. Ray, and P. Ring, Phys. Lett. B **726**, 680 (2013).
[47] A. V. Afanasjev and O. Abdurazakov, Phys. Rev. C **88**, 014320 (2013).
[48] S. Cwiok, P.-H. Heenen, and W. Nazarewicz, Nature (London) **433**, 705 (2005).

[49] K. Zhang, M.-K. Cheoun, Y.-B. Choi, P. S. Chong, J. Dong, Z. Dong, X. Du, L. Geng, E. Ha, X.-T. He, C. Heo, M. C. Ho, E. J. In, S. Kim, Y. Kim, C.-H. Lee, J. Lee, H. Li, Z. Li, T. Luo, J. Meng, M.-H. Mun, Z. Niu, C. Pan, P. Papakonstantinou, X. Shang, C. Shen, G. Shen, W. Sun, X.-X. Sun, C. K. Tam, Thaivayongnou, C. Wang, X. Wang, S. H. Wong, J. Wu, X. Wu, X. Xia, Y. Yan, R. W.-Y. Yeung, T. C. Yiu, S. Zhang, W. Zhang, X. Zhang, Q. Zhao, and S.-G. Zhou, At. Data Nucl. Data Tables **144**, 101488 (2022).

[50] V. Hellemans, R. Fossion, S. D. Baerdemacker, and K. Heyde, Phys. Rev. C **71**, 034308 (2005).

[51] S. G. Nilsson and I. Ragnarsson, *Shapes and Shells in Nuclear Structure* (Cambridge University Press, Cambridge, 1995).

[52] M. Ionescu-Bujor *et al.*, Phys. Rev. C **81**, 024323 (2010).

[53] L. Gaudefroy, J. M. Daugas, M. Hass, S. Grévy, C. Stodel, J. C. Thomas, L. Perrot, M. Girod, B. Rossé, J. C. Angélique, D. L. Balabanski, E. Fiori, C. Force, G. Georgiev, D. Kameda, V. Kumar, R. L. Lozeva, I. Matea, V. Méot, P. Morel, B. S. Nara Singh, F. Nowacki, and G. Simpson, Phys. Rev. Lett. **102**, 092501 (2009).

[54] J. Meng, *Relativistic Density Functional for Nuclear Structure* (World Scientific, Singapore, 2016).

[55] N. Nikolov, N. Schunck, W. Nazarewicz, M. Bender, and J. Pei, Phys. Rev. C **83**, 034305 (2011).

[56] I. Angeli and K. P. Marinova, At. Data Nucl. Data Tables **99**, 69 (2013).